



Multicenter Privacy-Preserving Model Training for Deep Learning Brain Metastases Autosegmentation

Yixing Huang^{a,d,e,*}, Zahra Khodabakhshi^b, Ahmed Gomaa^{a,d,e}, Manuel Schmidt^c, Rainer Fietkau^{a,d,e}, Matthias Guckenberger^b, Nicolaus Andratschke^b, Christoph Bert^{a,d,e}, Stephanie Tanadini-Lang^{b,*}, Florian Putz^{a,d,e}

^aDepartment of Radiation Oncology, Universitätsklinikum Erlangen, Friedrich-Alexander-Universität Erlangen-Nürnberg, Erlangen, Germany

^bDepartment of Radiation Oncology, University Hospital Zurich, University of Zurich, Zurich, Switzerland

^cDepartment of Neuroradiology, Universitätsklinikum Erlangen, Friedrich-Alexander-Universität Erlangen-Nürnberg, Erlangen, Germany

^dComprehensive Cancer Center Erlangen-EMN (CCC ER-EMN), Erlangen, Germany

^eBavarian Cancer Research Center (BZKF), Erlangen, Germany

ARTICLE INFO

Article history:

Keywords: Continual learning, Learning without forgetting, Brain metastasis, Multicenter collaboration, Data privacy, Data heterogeneity

ABSTRACT

Objectives: This work aims to explore the impact of multicenter data heterogeneity on deep learning brain metastases (BM) autosegmentation performance, and assess the efficacy of an incremental transfer learning technique, namely learning without forgetting (LWF), to improve model generalizability without sharing raw data.

Materials and methods: A total of six BM datasets from University Hospital Erlangen (UKER), University Hospital Zurich (USZ), Stanford, University of California San Francisco (UCSF), New York University (NYU) and Brain Tumor Segmentation (BraTS) Challenge 2023 on BM segmentation were used for this evaluation. First, the multicenter performance of a convolutional neural network (DeepMedic) for BM autosegmentation was established for exclusive single-center training and for training on pooled data, respectively. Subsequently bilateral collaboration was evaluated, where a UKER pretrained model is shared to another center for further training using transfer learning (TL) either with or without LWF.

Results: For single-center training, average F1 scores of BM detection range from 0.625 (NYU) to 0.876 (UKER) on respective single-center test data. Mixed multicenter training notably improves F1 scores at Stanford and NYU, with negligible improvement at other centers. When the UKER pretrained model is applied to USZ, LWF achieves a higher average F1 score (0.839) than naive TL (0.570) and single-center training (0.688) on combined UKER and USZ test data. Naive TL improves sensitivity and contouring accuracy, but compromises precision. Conversely, LWF demonstrates commendable sensitivity, precision and contouring accuracy. When applied to Stanford, similar performance was observed.

Conclusion: Data heterogeneity (e.g., variations in metastases density, metastases spatial distribution, and image spatial resolution across centers) results in varying performance in BM autosegmentation, posing challenges to model generalizability. LWF is a promising approach to peer-to-peer privacy-preserving model training.

1. Introduction

Individuals diagnosed with metastatic cancer face a significant likelihood of developing brain metastases (BM), with reported incidence rates reaching up to 40% [1]. The advent of BM often results in the diminished effectiveness of standard systemic therapies, underscoring the importance of effective BM management for improving patient survival and quality-of-life [2]. Given the cognitive deficits associated with whole-brain radiotherapy, stereotactic radiosurgery (SRS) has emerged as a preferred method for BM treatment [3, 4]. SRS administers precisely targeted radiation to the metastatic regions while sparing the adjacent healthy brain tissue, thereby minimizing side effects in comparison to whole-brain radiotherapy. The planning of SRS treatment necessitates detailed information on the number, size, locations, and boundaries of BM [5], which in turn requires their precise detection and contouring. At present, the identification of BM is predominantly a manual process conducted by neuroradiologists and radiation oncologists, which is not only time-intensive but also prone to variability between observers [6]. This manual identification process particularly fails with smaller metastases, which may go unnoticed due to their visibility on few image slices and their low contrast [6]. Moreover, the challenge of distinguishing BM from similar-looking anatomical structures, like blood vessels, in 2D image slices further complicates manual identification [7]. Although these smaller metastases might be detected in subsequent scans as they increase in size, initiating treatment at later stages can adversely impact patient outcomes, as larger metastases are harder to manage and often associated with more severe symptoms [8]. Consequently, the development of automated, computer-assisted techniques for BM identification holds significant importance for clinical practice.

With the fast development of deep learning techniques and their adoptions into the field of radiation oncology, many deep learning algorithms have been proposed for automatic BM detection and segmentation [9, 10], which have achieved high efficiency (compared with manual identification) and impressive efficacy despite of performance variance. According to the latest systematics reviews [9, 10], 3D U-Net [11, 12, 6, 13, 14, 15] and DeepMedic [16, 17, 18, 19] based networks are the most commonly used and effective networks for BM identification. Among all the reported methods, most of them were developed from and evaluated on single-center, in-house data, while multi-center studies are gaining more and more attention [11, 20, 6, 14, 15]. The performance of deep learning algorithms relies highly on the amount and quality of training data. Due to the limited data in a single center, multi-center collaboration is very important for developing high performance deep learning models. Nevertheless, the influence of data heterogeneity among multiple centers in deep learning auto-segmentation model performance has not yet been fully addressed.

In addition, due to data privacy and data management regu-

lations (e.g., the EU medical device regulation [21]), data sharing among multiple centers is restricted, which impedes the development of high performance deep learning tumor segmentation models from multicenter collaboration. To overcome the data privacy issue, federated learning, which trains a high performance model collaboratively without sharing data, has been proposed [22]. Due to the technical difficulty, communication frequency, financial cost and management complexity, center-to-peer federated learning [22], where a central server is required to coordinate training information for a global model, is challenging for practical use. Moreover, an implicit power hierarchy may arise from the centralized structure of center-to-peer federated learning, making cooperation unattractive for participating peer-level institutions. Therefore, peer-to-peer federated learning [22] is more feasible in practice, and the simplest way is to continually train the same model one center after another [23]. However, when a model is retrained on new datasets or tasks (i.e., naive transfer learning), deep learning suffers from the problem of catastrophic forgetting [24], i.e., deep learning models forget learned old knowledge catastrophically. Continual learning [24] aims to allow machine learning models to be updated through new data while retaining previously learned knowledge. In our in-depth technical survey [25] on 2D medical classification and segmentation tasks, learning without forgetting (LWF) [26] was superior to other regularization-based continual learning methods with statistical significance. Therefore, in this work, the efficacy of LWF in multicenter collaboration on BM auto-segmentation is investigated. With the public release of multiple BM datasets like the BraTS BM Challenge [27], such an investigation is feasible now.

This work aims to:

- Investigate the influence of data heterogeneity across multiple centers on the performance of deep learning models for BM autodetection.
- Assess the efficacy of LWF as a privacy-preserving strategy for multicenter collaboration in improving model generalizability.
- Evaluate the generalizability of the UKER single-center-training model and assess whether this UKER pretrained model enhances the generalizability of models for other centers.

2. Materials And Methods

2.1. Datasets

T1 contrast enhanced (T1CE) MRI datasets from University Hospital Erlangen (Universitätsklinikum, UKER), University Hospital Zurich (Universitäts Spital Zürich, USZ), Stanford University¹ [28], University of California San Francisco (UCSF)² [29], New York University (NYU)³ and Brain Tumor

*Corresponding authors: email: yixing.huang@uk-erlangen.de; stephanie.tanadini-lang@usz.ch

¹<https://aimi.stanford.edu/brainmetshare>

²<https://imagingdatasets.ucsf.edu/dataset/1>

³<https://nyumets.org/>

Table 1. Details of BM datasets from different centers.

Dataset	UKER	USZ	Stanford	UCSF	NYU	BraTS
# training volumes	600	157	56	200	104	178
# validation volumes	67	10	5	23	10	10
# test volumes	103	35	40	100	50	50
In-plane resolution (mm)	≤ 1.0	0.6	0.94	≤ 1.0	≤ 1.0	≤ 1.0
Through-plane slice thickness (mm)	≤ 1.0	0.6	1.0	≤ 1.5	≤ 5.0	≤ 5.0
# metastases per volume	2.2	4.2	12.2	10.3	6.6	7.8
# training metastases	1505	640	544	2159	616	1601
# validation metastases	130	29	33	357	102	35
# test metastases	272	144	656	826	359	213
Mean training metastasis size (cm ³)	1.642	1.506	0.352	0.327	0.828	1.371
Mean validation metastasis size (cm ³)	1.761	2.650	0.196	0.329	0.583	5.603
Mean test metastasis size (cm ³)	1.950	1.490	0.237	0.879	1.189	1.786
Median training metastasis size (cm ³)	0.132	0.229	0.054	0.034	0.078	0.073
Median validation metastasis size (cm ³)	0.216	0.402	0.067	0.038	0.077	0.070
Median test metastasis size (cm ³)	0.131	0.134	0.031	0.037	0.077	0.067
Training metastases ≤ 0.1 cm ³	44.4%	35.4%	67.5%	71.2%	55.5%	56.3%
Validation metastases ≤ 0.1 cm ³	36.9%	31.0%	60.6%	72.3%	57.8%	54.3%
Test metastases ≤ 0.1 cm ³	46.0%	44.4%	79.0%	67.4%	57.4%	55.9%

Segmentation (BraTS) 2023 BM Segmentation Challenge⁴ [27] were used for evaluation. The UKER and USZ datasets are internal, whereas the Stanford, UCSF, NYU and BraTS datasets are publicly available. Since T1CE is the main sequence used for radiotherapy treatment planning [30, 31, 32] and other sequences are missing in some datasets, in this work only T1CE volumes are used.

For the UKER and USZ data, ethical review and approval was not required for this study in accordance with the local legislation and institutional requirements. Written informed consent that data may be used for retrospective scientific studies was provided by the patients. Other datasets are publicly available. The data contributors have submitted Institutional Review Board (IRB) and Data Transfer Agreement (DTA) applications to their individual institution regulating bodies and obtained approval [28, 29, 27].

The UKER dataset contains 853 T1CE volumes in total using the MPRAGE sequence from a longitudinal study [33]. The volumes were acquired from various Siemens Healthcare 1.5 Tesla MRI scanners (Magnetom Aera and Magnetom Avanto mainly). The primary cancers include 41.3% skin cancer, 22.2% lung cancer, 12.4% breast cancer, and 10.5% kidney cancer. Among all the metastases, 44.9% are smaller than 0.1 cm³ (i.e., 100 voxels), which is approximately equivalent to a sphere with a radius of 3 mm. The USZ dataset contains 202 T1CE turbo field echo (TFE) volumes from a Philips Healthcare Ingenia 3.0 Tesla scanner. The primary cancers mainly include lung cancers and melanoma cancers. The details of other public datasets can be found in their respective descriptions [28, 29, 27]. The BM distribution of different datasets in size, density, and patient number are summarized

in Tab. 1. Each dataset is exclusively partitioned into training, validation, and test subsets, with all volumes from the same patient contained within a single subset. All the MRI volumes were preprocessed by the same pipeline: skull stripping, volume/voxel size uniformization, bias field correction, and intensity Z-normalization. All the volumes have 240 × 240 × 155 voxels with a voxel size of 1 mm × 1 mm × 1 mm.

Note that the total numbers of cases with labels accessible to public participants may differ from those reported in the dataset descriptions. For example, in the BraTS Challenge 238 labeled cases were released for training, and 31 unlabeled cases are available for validation, while the remaining 59 cases are not accessible to participants. Therefore, in this work, only 238 labeled cases were used instead of the 328 cases described in [27]. Due to intra- and inter-rater variations, annotations errors inevitably exist in the datasets. For example, Fig. 3(j) is an example of human annotation errors in the Stanford dataset, where the tiny metastasis indicated by the yellow arrow was not labeled and the annotation mask of the top metastasis is not accurate. In this work, the reference masks provided by the data providers without any further refinement were utilized. This ensures consistency when these datasets are employed by other researchers, thereby maintaining integrity and preventing potential biases.

2.2. Neural network and learning without forgetting

The DeepMedic network [34] is chosen because of its efficacy in various brain tumor segmentation tasks as well as its success in BM identification [34, 35, 36, 18, 37, 19]. For BM segmentation, class imbalance is a major issue as normal tissue voxels outnumber BM voxels. To overcome this problem, DeepMedic performs online sampling of training subvolumes/segments to keep class balance during training. In addition, multi-scale features are extracted via parallel convolu-

⁴<https://www.synapse.org/>

tional pathways. In our previous work [19], DeepMedic has achieved encouraging performance on the UKER dataset. In this work, the performance of DeepMedic on different datasets is evaluated.

In order to train a model from multiple centers without sharing raw data, peer-to-peer federated learning is one promising approach. The most straightforward way for such peer-to-peer federated learning involves continuous model training across various centers through weight transfer. Specifically, single weight transfer (SWT) sequentially trains the model from the first to the last center, whereas cyclic weight transfer (CWT) iteratively trains the model across all centers in cycles, as described in [38]. To avoid the forgetting problem after model sharing, continual learning techniques can be applied. In our previous in-depth survey [25], LWF was demonstrated to have superior performance to other continual learning regularization methods. Therefore, LWF is chosen in this work. LWF controls forgetting by imposing network output stability. In other words, the model trained with local data should yield similar predictions for specific samples as it did before training. Knowledge distillation loss (KDL) [39] is the key element of LWF, which constrains the new model (called student model) output to have a similar distribution of class probabilities to those predicted by the teacher model.

The objective function for LWF consists of a regular segmentation loss \mathcal{L}_{seg} and the KDL \mathcal{L}_{KDL} ,

$$\mathcal{L}_{\text{LWF}} = \mathcal{L}_{\text{seg}}(\mathcal{M}(\mathbf{x}, \theta), \mathbf{y}) + \lambda \mathcal{L}_{\text{KDL}}(\mathcal{M}(\mathbf{x}, \theta), \mathcal{M}(\mathbf{x}, \theta_0)), \quad (1)$$

where \mathcal{M} is the network model, \mathbf{x} is the set of input data samples and \mathbf{y} is the set of corresponding ground truth segmentation masks, λ is a relaxation parameter for KDL, θ_0 is the model parameter set from the previous center (teacher model), and θ is the current model parameter set to optimize.

All DeepMedic models were trained on an NVIDIA Quadro RTX 8000 GPU with Intel Xeon Gold 6158R CPUs. The model was trained for 300 epochs at each center. The validation was performed every two epochs, and the final models were selected based on the best validation performance (i.e., best volumetric Dice scores). The Adam optimizer with an initial learning rate of 0.001 and a weight decay of 0.0001 was applied. A probability of 50% for extracting tumor class containing segments was applied to keep class-balance. In this work, the binary cross-entropy (BCE) loss together with a subvolume-level sensitivity-specificity loss ($\alpha = 0.5$) [19] was used for \mathcal{L}_{seg} , and λ was set to 0.1 in Eqn. (1). Our implementation is publicly available on GitHub for further research and collaboration⁵.

2.3. Evaluation metrics

For detection performance, the lesion-wise sensitivity, precision, and average false positive rate (FPR) are used for the evaluation of BM identification accuracy. Sensitivity is defined as the number of true positive BM divided by the number of true positive plus false negative BM. Precision is defined as the number of true positive BM divided by the number of true positive

plus false positive BM. FPR is defined as the average number of false positive BM per patient volume. In this work, any segmentation demonstrating an overlap of at least one voxel with the reference label segmentation was considered a true positive (i.e., no overlap cutoff), since tiny BM contain only a few voxels and some comprise just a single voxel. Because of the trade-off between sensitivity and precision, F_β score is commonly used in many biomedical detection and segmentation tasks:

$$F_\beta = (1 + \beta^2) \cdot \frac{\text{sensitivity} \cdot \text{precision}}{\beta^2 \cdot \text{precision} + \text{sensitivity}}, \quad (2)$$

where a larger β parameter values sensitivity more than precision. In this work, F1 and F2 are used.

In clinical practice, true positive metastases are confirmed first and subsequently their contouring masks will be refined for treatment planning (i.e., **detection first and contouring later**) in a manual manner. Therefore, in this work, the contouring accuracy is evaluated on a per-lesion level for true positive metastases only. Because of partial volume effect, the exact reference boundary of small metastases is very challenging for human expert to determine (annotation errors, e.g., Fig. 3(j)). Conventional DSC is very sensitive to tiny errors for small metastases and Hausdorff distance is sensitive to outlier voxels. Therefore, the surface Dice (sDice) score [40] with a tolerance of 1 mm (compensate annotation errors) and 95% Hausdorff distance (HD95) are better metrics for clinical practice [41] to evaluate the contouring accuracy in this work. The definition of sDice is provided in Fig. 5 of [40], and HD95 is calculated as the 95th percentile of the distances between boundary points of two segmentation masks. Note that the conventional Dice scores and Hausdorff distances are reported in the supplementary tables. All the experiments were repeated 5 times and the unpaired t-test was used for assessing statistical significance.

3. Results

3.1. Qualitative data heterogeneity analysis

In addition to the BM distribution in Tab. 1, axial and coronal image examples from different centers are displayed in Fig. 1, where data heterogeneity is clearly observed:

a) BM density: The UKER dataset has the lowest density, whereas Stanford and UCSF have a high density.

b) BM spatial distribution: The USZ dataset includes metastases of leptomeningeal origin near cortical surfaces and meninges, while BM in other datasets are mainly located in the brain parenchyma.

c) Image resolution: Many cases in the NYU and BraTS datasets have low resolution along the transversal dimension (due to the use of older 2D T1 spin echo sequences), which increases the difficulty for human labeling as well as automatic detection.

d) Image contrast: The UCSF datasets contains much more cases where blood vessels and meninges are highly enhanced (e.g. related to higher contrast agent dose or lower time interval between contrast administration and sequence acquisition in the imaging protocols), which has the risk to increase false positive detection rate, e.g., the false positive structure in Fig. 1(d).

⁵<https://github.com/YixingHuang/DeepMedicPytorch>

Table 2. Autosegmentation performance on different datasets with single-center or mixed training (average from 5 repeats, lesion-wise, HD95 unit: mm).

Training	Test Data	Sensitivity	Precision	FPR	F1	F2	sDice	HD95
Single-center	UKER	0.854	0.900	0.25	0.876	0.863	0.790	4.21
	USZ	0.831	0.776 (0.367)	0.99 (6.06)	0.802 (0.506)	0.819 (0.659)	0.727	8.43
	Stanford	0.657	0.723	4.15	0.688	0.669	0.671	3.77
	UCSF	0.847	0.704	2.94	0.769	0.814	0.759	3.67
	NYU	0.714	0.557	4.11	0.625	0.675	0.600	8.61
	BraTS	0.769	0.575	2.17	0.658	0.720	0.595	6.79
Mixed (five centers without USZ)	UKER	0.906	0.814	0.55	0.857	0.886	0.880	2.75
	USZ	0.885	0.651	1.95	0.750	0.825	0.775	8.76
	Stanford	0.781	0.836	2.54	0.807	0.791	0.839	2.27
	UCSF	0.855	0.705	2.98	0.772	0.820	0.839	2.19
	NYU	0.764	0.649	2.98	0.702	0.738	0.767	5.55
	BraTS	0.867	0.445	4.64	0.587	0.728	0.689	5.83

Note: The values in brackets for USZ are without binary brain masks (brain masks can remove false positive metastases outside brain regions). Others have the same values for both with and without brain masks. The bold values highlight the centers, which have notable benefit in BM detection from mixed training compared with single-center training.

Table 3. Autosegmentation performance for bilateral collaboration using different training methods (average from 5 repeats, lesion-wise, HD95 unit: mm).

Training	Test Data	Model	Sensitivity	Precision	FPR	F1	F2	sDice	HD95
UKER+USZ collaboration	Combined UKER+USZ	USZ _{single-center}	0.839	0.584 (0.262)	1.81 (7.24)	0.688 (0.399)	0.771 (0.581)	0.755	5.36
		TL _{UKER⇒USZ}	0.905	0.418 (0.356)	3.89 (5.26)	0.570 (0.506)	0.732 (0.685)	0.821	4.63
		LWF _{UKER⇒USZ}	0.864	0.815	0.59	0.839	0.854	0.737	7.01
UKER+Stanford collaboration	Combined UKER+Stanford	Stanford _{single-center}	0.686	0.591	3.29	0.630	0.661	0.592	7.79
		TL _{UKER⇒Stanford}	0.854	0.455	6.66	0.593	0.726	0.823	2.77
		LWF _{UKER⇒Stanford}	0.763	0.811	1.16	0.786	0.772	0.779	3.51
		LWF _{UKER⇒Stanford, CWT}	0.796	0.708	2.15	0.749	0.776	0.798	3.13
		Mixed _{UKER+Stanford}	0.783	0.832	1.03	0.807	0.792	0.827	2.85

Note: The values in brackets are without binary brain masks (brain masks can remove false positive metastases outside brain regions). Others have the same values for both with and without brain masks. TL: transfer learning (TL) without LWF; LWF: transfer learning with LWF; CWT: cyclic weight transfer. The bold values highlight the best detection or contouring performances. USZ_{single-center} and Stanford_{single-center} were solely trained on USZ and Stanford data respectively and are provided as a reference.

3.2. Results of single-center training performance

The performance of single-center-training model is displayed in the top part of Tab. 2, where neither models nor raw data were shared. The UKER model achieves a relatively high lesion-wise sensitivity and precision, potentially due to the high image quality, low metastasis density, and a large number of training volumes. The UCSF model achieves a similar sensitivity, but with a slightly lower precision. The Stanford model achieves a low sensitivity, due to the small number of training patients. In contrast, the NYU and BraTS models achieved low precision values on their respective test data, which could be ascribed to their low axial slice resolution.

As the USZ dataset includes metastases of leptomeningeal origin near cortical surfaces and meninges, the trained model predicted many false positive metastases (5.1 metastases per patient on average) outside the brain region, e.g., Fig. 3(b) and Fig. 3(e). This behavior is only observed for models trained from the USZ dataset, but serves as a good indicator of model performance and knowledge transferability. Such false positive metastases can be simply removed with binary brain masks

(no brain masks were used in the input data in this work to save computation), and the precision is improved from 0.367 to 0.776.

The single-center training performances of UKER and UCSF models with respect to training data amount are displayed in Fig. 2(a) and (b), respectively. With limited training data, the model tends to focus on obvious, large metastases. As the training data expands, the model learns from a broader spectrum of examples and starts to detect challenging, small metastases. Therefore, with the increase of training data, precision oscillates (for UKER) or drops (for UCSF). In contrast, sensitivity increases monotonically for both UKER and UCSF. As a result, F2 scores increase monotonically for both UKER and UCSF, whereas the F1 score for UCSF oscillates. Therefore, in this work, we choose F2 as the main detection metric instead of F1. With the increasing amount of training data, the contouring accuracy of true positive metastases increases monotonically.

3.3. Results of mixed multicenter training

When the training data of UKER, Stanford, UCSF, NYU and BraTS are mixed to train a joint model (USZ training data was not mixed due to data privacy), its performance on different test datasets are displayed in the bottom part of Tab 2. Compared to single-center training, mixed training demonstrates improved detection sensitivity across all centers, with statistically significant ($p \leq 0.0058$) gains at all centers except UCSF. The F2 scores of Stanford and NYU have a significant improvement ($p \leq 0.0001$) and the F2 score of UKER has a considerable improvement ($p = 0.0145$), as displayed in Fig. 2(c). This is consistent with the expectation that more training data leads to better detection performance.

However, USZ, UCSF and BraTS with mixed training have similar F2 scores to those with single-center training, respectively, as displayed in Fig. 2(c). **This observation indicates that more training data from other centers does not necessarily improve BM detection performance, which can be attributed to the data heterogeneity among different centers.**

Nevertheless, the mixed-training model achieved considerably better contouring performance for true positive metastases than single-center-training models, as displayed in Tab. 2 and Fig. 2(d). The sDice scores of mixed training are significantly ($p \leq 0.0001$) better than those of single-center training at all centers except USZ.

3.4. Results of UKER model shared to USZ

The results of the bilateral collaboration between UKER and USZ are reported in Tab. 3 (overall performance on both test datasets) as well as supplementary Tab. 2 (performance on each individual test dataset).

Single-center training: When the UKER pretrained model was directly applied to USZ test data without further fine-tuning, the model achieved decent sensitivity and precision without brain masks (see Supplementary Tab. 2). Even when no brain masks were used, no false positive metastases were predicted outside the brain region. However, when the USZ pretrained model was directly applied to UKER test data, the model obtained a decent sensitivity but a very low precision. **This indicates the good generalizability of the UKER model to the USZ data, whereas the reverse scenario—applying the model from USZ to UKER data—does not possess comparable generalizability.**

Naive transfer learning (TL): When the UKER model was fine-tuned without LWF on USZ training dataset, the naive TL model achieved high sensitivity (0.915) but low precision (0.362) for the UKER test data. The TL model predicted false positive metastases near the brain boundary for both USZ and UKER data (some examples displayed in Fig. 3(c)-(h)). **These results reveal that the fine-tuned model overfits to the USZ data and forgets the knowledge learned from the UKER data.**

LWF: However, when LWF was used for fine-tuning, the LWF model achieved decent sensitivity (0.822) and precision (0.730) without brain mask for the USZ test data. No false positive metastases were predicted outside the brain region, **indicating the benefit of LWF in the target center.** The LWF model

achieved high sensitivity (0.874) and high precision (0.855) on the UKER test data (one example in Fig. 3(d)), **demonstrating the learned knowledge from the UKER training dataset was preserved.**

Overall comparison: Regarding the overall performance on both test datasets (Tab. 3), the USZ single-center-training model and the TL model achieved low F2 scores with brain masks, respectively. In contrast, **the LWF model achieved the best F2 score of 0.854, which is significantly better than USZ single-center training and TL ($p \leq 0.0001$).** This highlights the benefit of LWF in privacy-preserving bilateral collaboration for BM detection. Although TL is not optimal for BM detection, it is beneficial to improve BM contouring accuracy of true positive metastases (sDice significant with $p \leq 0.0001$), as indicated by Fig. 2(e).

3.5. Results of UKER model shared to Stanford

The bilateral collaboration between UKER and Stanford was performed as well. The main differences between the UKER and Stanford datasets are the BM density as well as BM size and the number of training patients. The Stanford single-center-training model got low sensitivity and low precision on the combined UKER and Stanford test data, because of the low number of training data. The TL model has a significantly large improvement in detection sensitivity ($p \leq 0.0001$) and contouring accuracy ($p \leq 0.0001$). But it has a very low detection precision ($p = 0.0282$). Likely the TL model tends to overestimate the presence of BM in the UKER test data due to the high BM density in the Stanford training data, leading to a high number of false positives. The LWF model achieved both good sensitivity and precision, and hence has a significantly better F2 score of 0.772 than single-center training ($p \leq 0.0001$) and TL ($p \leq 0.0003$), which is close to that of mixed training ($F2 = 0.792$, $p = 0.0103$).

To check whether CWT is beneficial, 4 iterations of weight transfers was performed. Compared with single weight transfer (SWT), CWT with LWF further improves the segmentation accuracy (sDice from 0.779 to 0.798, HD95 from 3.51 mm to 3.13 mm), but no statistical significance was found.

4. Discussion

In general, F1 is the most widely used F_β score in medical classification/segmentation tasks. For BM detection, the first primary clinical requirement is to correctly detect the existence of BM with high sensitivity irrespective of the exact 3D extent of each metastasis. False positive BM can be removed afterwards by human expert review. In practice, achieving a high sensitivity is more challenging than achieving a high precision for a deep learning model. For example, a high precision can be easily obtained by a network if it only detects a few large, high-contrast BM (which are easy) without false positives, but it is very challenging to detect all the metastases (large and small, high and low contrast). **Therefore, F2, which emphasizes sensitivity more than precision, is more appropriate than F1 as the BM detection metric for clinical application [41]. Fig. 2 (and the average detection performance of Tab. 2 in [29])**

as well) demonstrates the advantage of F2 over F1 with increasing training data amount. It is worth mentioning that the advantage of LWF over TL and single-center training is more prominent in F1 than F2, as displayed in Tab. 3.

The single-center training shows that Stanford, NYU and BraTS had low F2 scores. With mixed training, the F2 score of Stanford was improved. However, those of NYU and BraTS stayed low despite of improvement. This is very likely because of their distinct image features from other datasets, in particular the low axial slice resolution. **This implies that deep learning models for BM identification also require high image quality similar to human experts.** For human experts, ≤ 1 mm isotropic resolution on 3D scans has become a consensus of image resolution requirement among radiation oncology communities [31, 30]. Human experts have also reached consensus on optimal sequence selection, contrast agent uptake, distortion correction, and motion control [30]. Satisfying such requirements are believed to improve deep learning model performance for BM identification as well.

The results on the UKER-USZ and UKER-Stanford collaborations show that TL can improve the sensitivity of the model as well as the segmentation accuracy of true positive metastases compared with single-center training, but the TL model tends to overfit to the target center data and detects more false positive BM. Further comparing LWF with TL, LWF can achieve relatively high sensitivity as well as high precision. This indicates that LWF is a promising approach for peer-to-peer federated learning and multicenter collaboration on BM autosegmentation without sharing raw data.

Several multicenter studies on deep learning for BM autosegmentation have been published previously [14, 11, 20, 15, 42, 43]. In contrast to the AURORA multicenter study, which reported a median BM volume size of 7.3 cm^3 , the datasets in our study feature significantly smaller median volume sizes, all less than 0.5 cm^3 . The principal novelty of our work lies in the introduction of a privacy-preserving method, i.e. LWF, which enables the training of a model across multiple centers without the need to share raw data. This contrasts with other studies, which typically rely on pooled multicenter data for model training. This approach addresses significant privacy concerns and enhances the feasibility of multicenter collaboration on BM autosegmentation.

The proposed LWF method generally exhibits robustness to parameter selection. The parameter λ in Eqn. 1 governs the balance between stability and plasticity [24]. A high λ value results in minimal model alterations at the target center, maintaining stability, whereas a low λ value aligns the model's performance more closely with that achieved by naive TL. Our experiments suggest that a λ range from 0.01 to 0.5 effectively balances stability and plasticity, with 0.1 identified as the optimal value. To facilitate effective multicenter collaboration, it is crucial that datasets from different centers undergo the same preprocessing steps, as detailed in Section 2.1. This standardization ensures consistency across centers, enhancing the overall efficacy of the collaboration and ultimately improving model generalizability.

This work has several limitations that should be noted: a) The training of 3D models requires significant computational

resources, which limited us to only five repetitions for each experimental setting. Ideally, a greater number of repetitions would be conducted to enhance the statistical robustness of the results. b) Although six datasets from different centers were available for this study, this offers numerous potential combinations for multicenter collaboration. However, we only investigated two bilateral collaboration scenarios to demonstrate the benefits of LWF. We plan to explore additional combinations and collaboration models in our future work to further validate and expand on these initial findings.

In addition to further combinations of datasets in this work, future studies will aim to include a wider variety of datasets from different hospitals and institutions across Europe. This would test the model's robustness and ability to generalize across diverse patient demographics and equipment variations. The ultimate goal is to seamlessly integrate the method in this work into existing clinical workflows. Achieving this integration necessitates comprehensive AI-specific quality assurance (QA) measures [44] to ensure the reliability, accuracy, and safety of the model. Prior to clinical deployment, the model must undergo stringent validation and secure approval from relevant health authorities, such as the Food and Drug Administration (FDA) or European Medicines Agency (EMA), confirming its safety and efficacy within clinical environments. Significant additional research will be necessary to bridge the gap between the developmental phase of this deep learning model for BM autosegmentation and its practical clinical application, ensuring that all scientific, regulatory, and operational benchmarks are met.

5. Conclusion

The heterogeneity of data across multiple centers poses a significant challenge to the generalizability of deep learning models from one center to another. This is particularly evident in the development of deep learning models for BM identification, which, akin to human experts, necessitate high-quality imaging data for both training and testing. TL and LWF emerge as valuable strategies for fostering privacy-preserving collaborations in the advancement of BM autosegmentation models. While TL demonstrates notable strengths in achieving high detection sensitivity and contouring accuracy, it does so at the expense of precision. Conversely, LWF presents a commendable equilibrium between sensitivity and precision, offering a more balanced approach to multicenter model development.

References

- [1] E. Tabouret, O. Chinot, P. Metellus, A. Tallet, P. Viens, A. Goncalves, Recent trends in epidemiology of brain metastases: an overview, *Anticancer Res.* 32 (11) (2012) 4655–4662.
- [2] E. Le Rhun, M. Guckenberger, M. Smits, R. Dummer, T. Bachelot, F. Sahm, N. Galldiks, E. de Azambuja, A. Berghoff, P. Metellus, et al., EANO–ESMO clinical practice guidelines for diagnosis, treatment and follow-up of patients with brain metastasis from solid tumours, *Ann. Oncol.* (2021).
- [3] M. Kocher, A. Wittig, M. D. Piroth, H. Treuer, H. Seegenschmiedt, M. Ruge, A.-L. Grosu, M. Guckenberger, Stereotactic radiosurgery for treatment of brain metastases, *Strahlenther. Onkol.* 190 (6) (2014) 521–532.

- [4] S. Rogers, B. Baumert, O. Blanck, D. Böhmer, J. Boström, R. Engenhart-Cabillic, E. Ermis, S. Exner, M. Guckenberger, D. Habermehl, et al., Stereotactic radiosurgery and radiotherapy for resected brain metastases: current pattern of care in the radiosurgery and stereotactic radiotherapy working group of the german association for radiation oncology (DEGRO), *Strahlentherapie und Onkologie* 198 (10) (2022) 919–925.
- [5] T. Welzel, R. A. El Shafie, B. v. Nettelblatt, D. Bernhardt, S. Rieken, J. Debus, Stereotactic radiotherapy of brain metastases: clinical impact of three-dimensional SPACE imaging for 3T-MRI-based treatment planning, *Strahlentherapie und Onkologie* 198 (10) (2022) 926–933.
- [6] J. Xue, B. Wang, Y. Ming, X. Liu, Z. Jiang, C. Wang, X. Liu, L. Chen, J. Qu, S. Xu, et al., Deep learning–based detection and segmentation-assisted management of brain metastases, *Neuro Oncol.* 22 (4) (2020) 505–514.
- [7] M. Kocher, M. I. Ruge, N. Galldiks, P. Lohmann, Applications of radiomics and machine learning for radiotherapy of malignant brain tumors, *Strahlenther. Onkol.* 196 (2020) 856–867.
- [8] A. M. Baschnagel, K. D. Meyer, P. Y. Chen, D. J. Krauss, R. E. Olson, D. R. Pieper, A. H. Maitz, H. Ye, I. S. Grills, Tumor volume as a predictor of survival and local control in patients with brain metastases treated with gamma knife surgery, *Journal of neurosurgery* 119 (5) (2013) 1139–1144.
- [9] T.-W. Wang, M.-S. Hsu, W.-K. Lee, H.-C. Pan, H.-C. Yang, C.-C. Lee, Y.-T. Wu, Brain metastasis tumor segmentation and detection using deep learning algorithms: a systematic review and meta-analysis, *Radiotherapy and Oncology* (2023) 110007.
- [10] B. B. Ozkara, M. M. Chen, C. Federau, M. Karabacak, T. M. Briere, J. Li, M. Wintermark, Deep learning for detecting brain metastases on MRI: a systematic review and meta-analysis, *Cancers* 15 (2) (2023) 334.
- [11] J. A. Buchner, F. Kofler, L. Etzel, M. Mayinger, S. M. Christ, T. B. Brunner, A. Wittig, B. Menze, C. Zimmer, B. Meyer, et al., Development and external validation of an MRI-based neural network for brain metastasis segmentation in the AURORA multicenter study, *Radiotherapy and Oncology* 178 (2023) 109425.
- [12] S. T. Jünger, U. C. I. Hoyer, D. Schaufler, K. R. Laukamp, L. Goertz, F. Thiele, J.-P. Grunz, M. Schlamann, M. Perkuhn, C. Kabbasch, et al., Fully automated MR detection and segmentation of brain metastases in non-small cell lung cancer using deep learning, *Journal of Magnetic Resonance Imaging* 54 (5) (2021) 1608–1622.
- [13] I. Pflüger, T. Wald, F. Isensee, M. Schell, H. Meredig, K. Schlamp, D. Bernhardt, G. Brugnara, C. P. Heußel, J. Debus, et al., Automated detection and quantification of brain metastases on clinical MRI data using artificial neural networks, *Neuro-oncology advances* 4 (1) (2022) vdacl38.
- [14] S. Yin, X. Luo, Y. Yang, Y. Shao, L. Ma, C. Lin, Q. Yang, D. Wang, Y. Luo, Z. Mai, et al., Development and validation of a deep-learning model for detecting brain metastases on 3D post-contrast MRI: a multi-center multi-reader evaluation study, *Neuro-oncology* 24 (9) (2022) 1559–1570.
- [15] J. A. Ottesen, D. Yi, E. Tong, M. Iv, A. Latysheva, C. Saxhaug, K. D. Jacobsen, Å. Helland, K. E. Emblem, D. L. Rubin, et al., 2.5d and 3d segmentation of brain metastases with deep learning on multinational MRI data, *Frontiers in Neuroinformatics* 16 (2023) 1056068.
- [16] A. T. Fairchild, J. K. Salama, W. F. Wiggins, B. G. Ackerson, P. E. Fecci, J. P. Kirkpatrick, S. R. Floyd, D. J. Godfrey, A deep learning-based computer aided detection (CAD) system for difficult-to-detect brain metastases, *International Journal of Radiation Oncology* Biology* Physics* 115 (3) (2023) 779–793.
- [17] L. Pennig, R. Shahzad, L. Caldeira, S. Lennartz, F. Thiele, L. Goertz, D. Zopfs, A.-K. Meißner, G. Fürtjes, M. Perkuhn, et al., Automated detection and segmentation of brain metastases in malignant melanoma: evaluation of a dedicated deep learning model, *American Journal of Neuroradiology* 42 (4) (2021) 655–662.
- [18] O. Charron, A. Lallemand, D. Jarnet, V. Noblet, J.-B. Clavier, P. Meyer, Automatic detection and segmentation of brain metastases on multimodal MR images with a deep convolutional neural network, *Comput. Biol. Med.* 95 (2018) 43–54.
- [19] Y. Huang, C. Bert, P. Sommer, B. Frey, U. Gaipl, L. V. Distel, T. Weissmann, M. Uder, M. A. Schmidt, A. Dörfner, et al., Deep learning for brain metastasis detection and segmentation in longitudinal mri data, *Medical Physics* 49 (9) (2022) 5773–5786.
- [20] J. Qu, W. Zhang, X. Shu, Y. Wang, L. Wang, M. Xu, L. Yao, N. Hu, B. Tang, L. Zhang, et al., Construction and evaluation of a gated high-resolution neural network for automatic brain metastasis detection and segmentation, *European Radiology* (2023) 1–11.
- [21] R. Beckers, Z. Kwade, F. Zanca, The EU medical device regulation: Implications for artificial intelligence-based medical device software in medical physics, *Phys. Med.* 83 (2021) 1–8.
- [22] J. Xu, B. S. Glicksberg, C. Su, P. Walker, J. Bian, F. Wang, Federated learning for healthcare informatics, *J. Healthc. Inform. Res.* 5 (1) (2021) 1–19.
- [23] M. J. Sheller, B. Edwards, G. A. Reina, J. Martin, S. Pati, A. Kotrotsou, M. Milchenko, W. Xu, D. Marcus, R. R. Colen, et al., Federated learning in medicine: facilitating multi-institutional collaborations without sharing patient data, *Scientific reports* 10 (1) (2020) 12598.
- [24] M. Delange, R. Aljundi, M. Masana, S. Parisot, X. Jia, A. Leonardis, G. Slabaugh, T. Tuytelaars, A continual learning survey: Defying forgetting in classification tasks, *IEEE Trans. Pattern Anal. Mach. Intell.* 1 (2021) 1–20.
- [25] Y. Huang, C. Bert, A. Goma, R. Fietkau, A. Maier, F. Putz, A survey of incremental transfer learning: Combining peer-to-peer federated learning and domain incremental learning for multicenter collaboration, *arXiv preprint arXiv:2309.17192* (2023) 1–16.
- [26] Z. Li, D. Hoiem, Learning without forgetting, *IEEE Trans. Pattern Anal. Mach. Intell.* 40 (12) (2017) 2935–2947.
- [27] A. W. Moawad, A. Janas, U. Baid, D. Ramakrishnan, L. Jekel, K. Krantchev, H. Moy, R. Saluja, K. Osenberg, K. Wilms, et al., The brain tumor segmentation (BraTS-METS) challenge 2023: Brain metastasis segmentation on pre-treatment mri, *ArXiv* (2023) 1–16.
- [28] E. Grøvik, D. Yi, M. Iv, E. Tong, D. Rubin, G. Zaharchuk, Deep learning enables automatic detection and segmentation of brain metastases on multisequence MRI, *J. Magn. Reson. Imaging* 51 (1) (2020) 175–182.
- [29] J. D. Rudie, R. S. D. A. Weiss, P. Nedelec, E. Calabrese, J. B. Colby, B. Laguna, J. Mongan, S. Braunstein, C. P. Hess, A. M. Rauschecker, et al., The University of California San Francisco, brain metastases stereotactic radiosurgery (UCSF-BMSR) MRI dataset, *arXiv preprint arXiv:2304.07248* (2023) 1–18.
- [30] F. Putz, M. Bock, D. Schmitt, C. Bert, O. Blanck, M. I. Ruge, E. Hattin-gen, C. P. Karger, R. Fietkau, J. Grigo, et al., Quality requirements for MRI simulation in cranial stereotactic radiotherapy: a guideline from the german taskforce “imaging in stereotactic radiotherapy”, *Strahlentherapie und Onkologie* (2024) 1–18.
- [31] T. J. Kaufmann, M. Smits, J. Boxerman, R. Huang, D. P. Barboriak, M. Weller, C. Chung, C. Tsien, P. D. Brown, L. Shankar, et al., Consensus recommendations for a standardized brain tumor imaging protocol for clinical trials in brain metastases, *Neuro-oncology* 22 (6) (2020) 757–772.
- [32] J. A. Buchner, J. C. Peeken, L. Etzel, I. Ezhov, M. Mayinger, S. M. Christ, T. B. Brunner, A. Wittig, B. H. Menze, C. Zimmer, et al., Identifying core MRI sequences for reliable automatic brain metastasis segmentation, *Radiotherapy and Oncology* 188 (2023) 109901.
- [33] F. Putz, T. Weissmann, D. Oft, M. A. Schmidt, J. Roesch, H. Siavoosh-haghighi, I. Filimonova, C. Schmitter, V. Mengling, C. Bert, et al., FSRT vs. SRS in brain metastases—differences in local control and radiation necrosis—a volumetric study, *Front. Oncol.* 10 (2020).
- [34] K. Kamnitsas, C. Ledig, V. F. Newcombe, J. P. Simpson, A. D. Kane, D. K. Menon, D. Rueckert, B. Glocker, Efficient multi-scale 3D CNN with fully connected CRF for accurate brain lesion segmentation, *Med. Image Anal.* 36 (2017) 61–78.
- [35] Y. Liu, S. Stojadinovic, B. Hrycushko, Z. Wardak, S. Lau, W. Lu, Y. Yan, S. B. Jiang, X. Zhen, R. Timmerman, et al., A deep convolutional neural network-based automatic delineation strategy for multiple brain metastases stereotactic radiosurgery, *PLoS One* 12 (10) (2017) e0185844.
- [36] S. Lu, S. Hu, W. Weng, Y. Chen, J. Lu, F. Xiao, F. Hsu, Automated detection and segmentation of brain metastases in stereotactic radiosurgery using three-dimensional deep neural networks, *Int. J. Radiat. Oncol. Biol. Phys.* 105 (1) (2019) S69–S70.
- [37] S.-Y. Hu, W.-H. Weng, S.-L. Lu, Y.-H. Cheng, F. Xiao, F.-M. Hsu, J.-T. Lu, Multimodal volume-aware detection and segmentation for brain metastases radiosurgery, in: *Proc. AIRT, Springer*, 2019, pp. 61–69.
- [38] K. Chang, N. Balachandar, C. Lam, D. Yi, J. Brown, A. Beers, B. Rosen, D. L. Rubin, J. Kalpathy-Cramer, Distributed deep learning networks among institutions for medical imaging, *Journal of the American Medical Informatics Association* 25 (8) (2018) 945–954.
- [39] G. Hinton, O. Vinyals, J. Dean, Distilling the knowledge in a neural net-

- work, in: NIPS Deep Learning and Representation Learning Workshop, 2015, pp. 1–9.
- [40] S. Nikolov, S. Blackwell, A. Zverovitch, R. Mendes, M. Livne, J. De Fauw, Y. Patel, C. Meyer, H. Askham, B. Romera-Paredes, et al., Clinically applicable segmentation of head and neck anatomy for radiotherapy: deep learning algorithm development and validation study, *Journal of medical Internet research* 23 (7) (2021) e26151.
- [41] L. Maier-Hein, A. Reinke, P. Godau, M. D. Tizabi, F. Buettner, E. Christodoulou, B. Glocker, F. Isensee, J. Kleesiek, M. Kozubek, et al., Metrics reloaded: recommendations for image analysis validation, *Nature methods* (2024) 1–18.
- [42] A. Liew, C. C. Lee, V. Subramaniam, B. L. Lan, M. Tan, Gradual self-training via confidence and volume based domain adaptation for multi dataset deep learning-based brain metastases detection using nonlocal networks on MRI images, *Journal of Magnetic Resonance Imaging* 57 (6) (2023) 1728–1740.
- [43] D. Bouget, A. Pedersen, A. S. Jakola, V. Kavouridis, K. E. Emblem, R. S. Eijgelaar, I. Kommers, H. Ardon, F. Barkhof, L. Bello, et al., Preoperative brain tumor imaging: Models and software for segmentation and standardized reporting, *Frontiers in neurology* 13 (2022) 932219.
- [44] M. Claessens, C. S. Oria, C. L. Brouwer, B. P. Ziemer, J. E. Scholey, H. Lin, A. Witzum, O. Morin, I. El Naqa, W. Van Elmpt, et al., Quality assurance for ai-based applications in radiation therapy, in: *Seminars in radiation oncology*, Vol. 32, Elsevier, 2022, pp. 421–431.

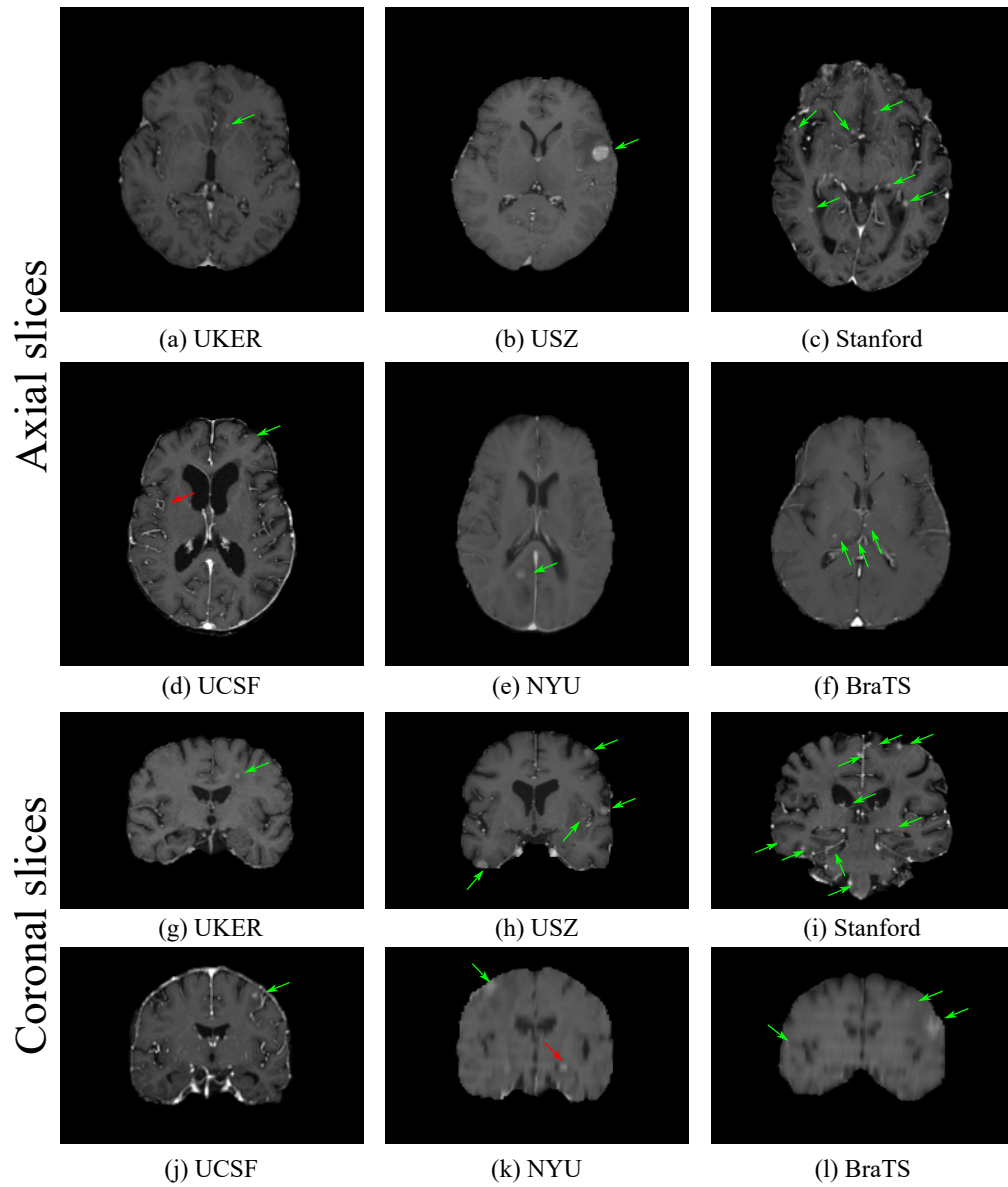


Fig. 1. Exemplary images from different datasets (top: axial slices; bottom: coronal slices). The axial and coronal slices of the same center are not from the same patients. The green arrows indicate true positive brain metastases, and the red arrows indicate suspicious spots which are true negative.

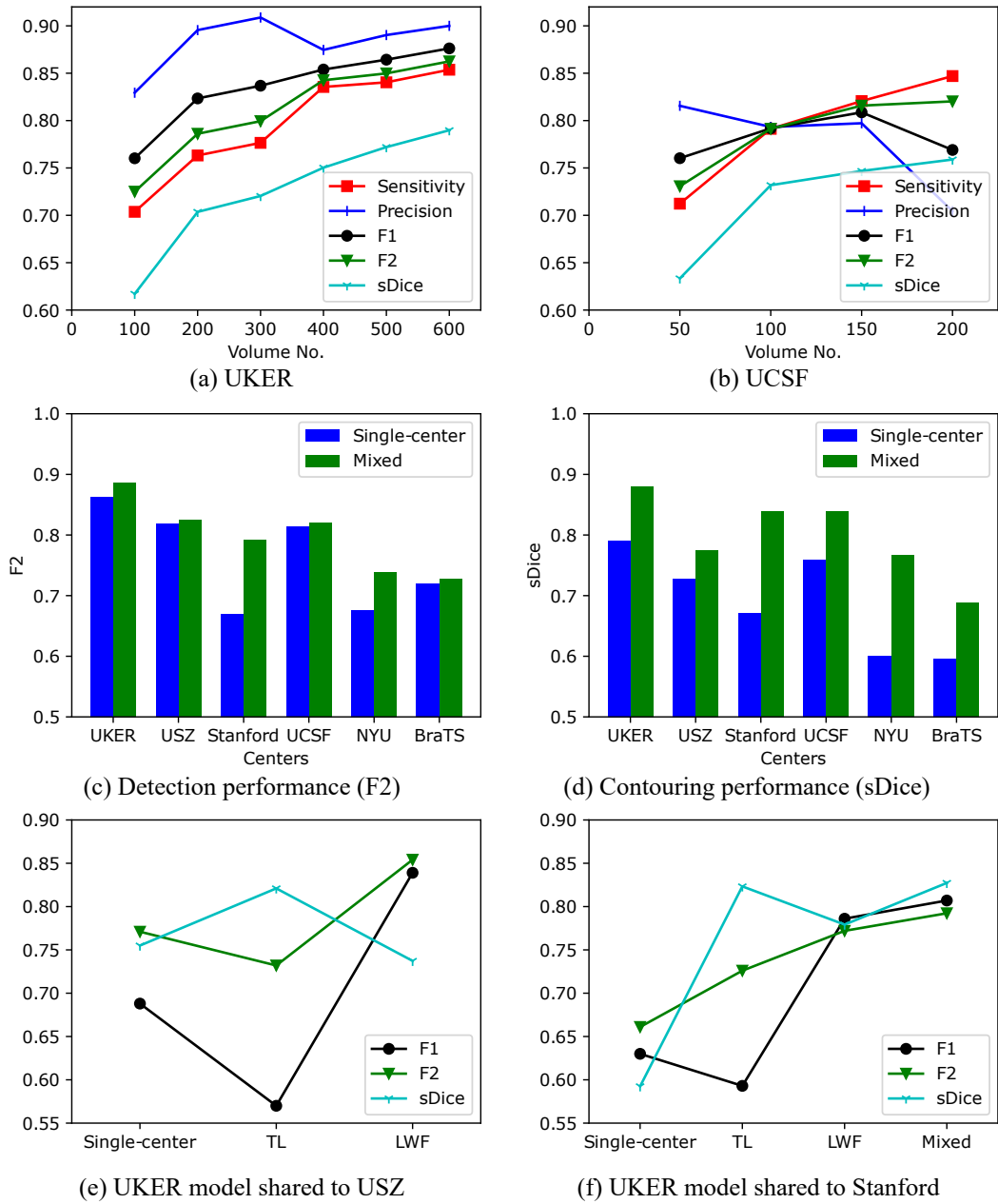


Fig. 2. The BM detection and segmentation performances of different models. (a) and (b) are the performances of UKER and UCSF single-center-training models with respect to training data amount (number of volumes/patients), respectively. (c) and (d) display the BM detection performance and segmentation performance respectively with single-center training and mixed training. (e) and (f) display BM detection and segmentation performances of different methods.

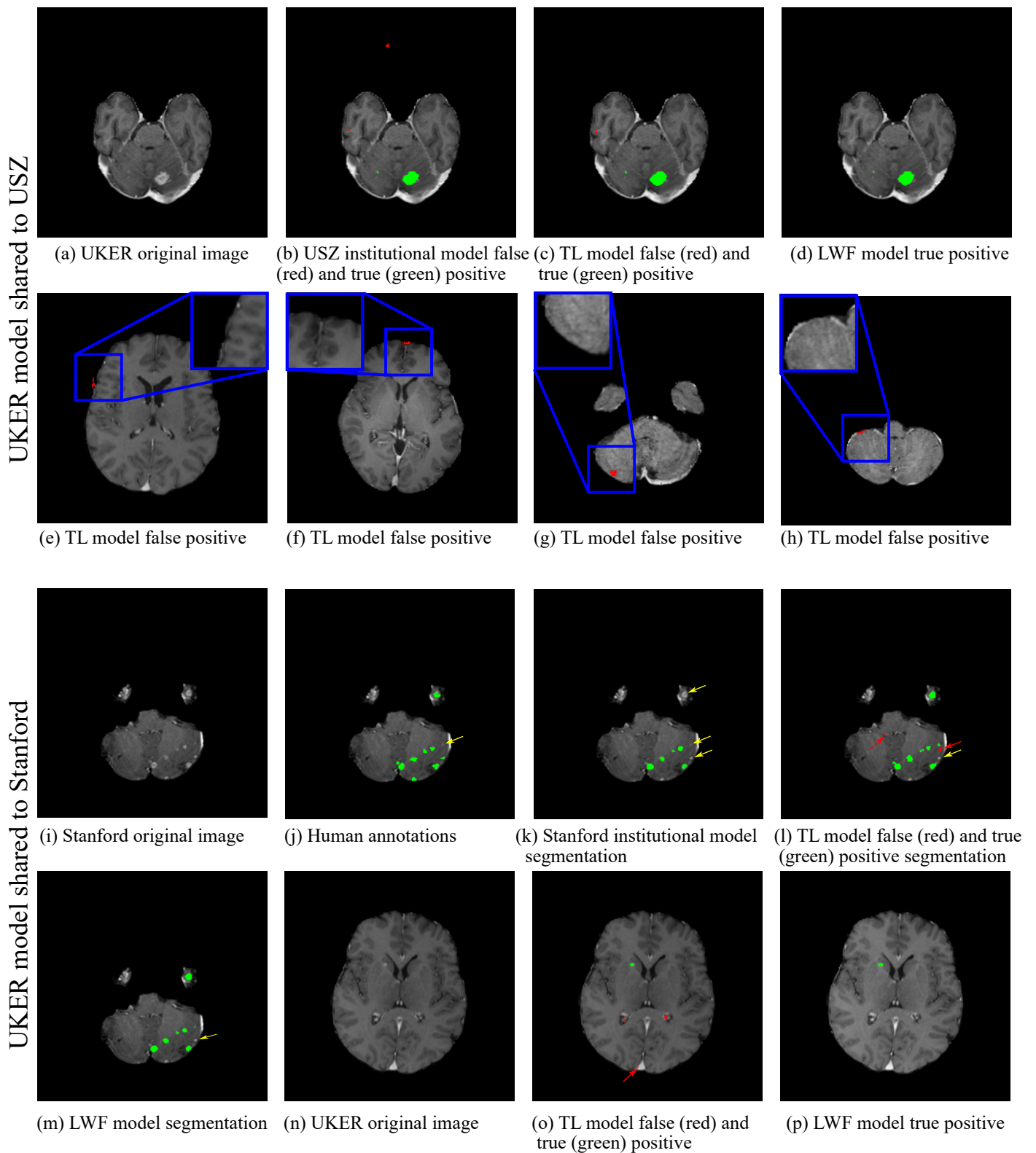


Fig. 3. The BM autosegmentation examples of different models. The top rows displays the results of different models on one UKER exemplary image when the UKER model was shared to USZ, while the second rows displays other representative false positive examples of the $TL_{UKER=USZ}$ model. The bottom two rows display the results of different models when the UKER model was shared to Stanford. Red areas are false positive segmentations, green areas are true positive segmentations, and the yellow arrows indicate false negative metastases. Subfigure (j) is an example of human annotation errors in the Stanford dataset, where the tiny metastasis indicated by the yellow arrow was not labeled, and the annotation mask of the top metastasis is not accurate.